UCRL--102499

DE90 006927

TIME-DEPENDENT TWO-DIMENSIONAL RADIATION HYDRODYNAMICS OF ACCRETING MATTER ONTO HIGHLY MAGNETIZED NEUTRON STARS

Richard I. Klein[1,2,3] and Jonathan Arons[1,3,4]

[1]Department of Astronomy, University of California at Berkeley; [2]Lawrence Livermore National Laboratory and [3]Institute of Geophysics and Planetary Physics, [4]Service d'Astrophysique CEN-Saclay

Invited Talk to be published in
23rd ESLAB Symposium on Two Topics in X-ray Astronomy
ESA SP-296

MASTER

DISTRIBUTION OF THIS DOCUMENT IS UNLIMITED

TIME-DEPENDENT TWO-DIMENSIONAL RADIATION HYDRODYNAMICS OF ACCRETING MATTER ONTO HIGHLY MAGNETIZED NEUTRON STARS

Richard I. Klein[1,2,3] and Jonathan Arons[1,3,4]

[1]Department of Astronomy, University of California, Berkeley; [2]Lawrence Livermore National Laboratory and [3]Institute of Geophysics and Planetary Physics, [4]Service d'Astrophysique CEN-Saclay

ABSTRACT

We present for the first time, the self-consistent solution of the two-dimensional, time-dependent equations of radiation-hydrodynamics governing the accretion of matter onto the highly magnetized polar caps of luminous x-ray pulsars. The calculations show a structure in the accretion column very different from previous one-zone uniform models. We have included all the relevant magnetic field corrections to both the hydrodynamics and the radiative transport. We include a new theory for the diffusion and advection of both radiation energy density and photon number density. For initially uniformly accreting models with super-Eddington flows, we have uncovered evidence of strong radiation-driven outflowing optically thin radiation filled regions of the accretion column embedded in optically-thick inflowing plasma. The development of these photon "bubbles" have growth times on the order of a millisecond and show fluctuations on sub-millisecond timescales. The photon bubbles are likely to be a consequence of convective over-stability and may result in observable fluctuations in the emitted luminosity leading to luminosity dependent changes in the pulse profile. This may provide important new diagnostics for conditions in accreting x-ray pulsars.

1. INTRODUCTION

The flow of fully ionized plasma onto the magnetic polar caps of a strongly magnetized neutron star is well accepted as the basic model for the pulsing x-ray sources in binary systems (Ref. 1, 2, 3). A great deal of observational evidence supports this picture. The basic hard x-ray spectrum is essentially consistent with the small polar cap area expected from accretion onto magnetized neutron stars, while the quasi-exponential roll-off observed in the spectra of many neutron stars at high energy are consistent with the interpretation of the spectrum as being due to the emission from a hot plasma with a Maxwellian distribution of radiating particles.

While the basic picture appears sound, several problems remain. There is to date no quantitative self-consistent interpretation of the spectra; the observed continua appear too flat at low frequencies; there have been only two x-ray pulsars with observed cyclotron lines and the problem of the beaming pattern has lacked a solution based on the physics of the flow. Most of the effort over the past decade has focused on studies of the detailed physical processes applied to one-zone uniform models (Ref. 4) where the emitting medium is treated as either a uniform slab or cylinder (Ref. 5). These models have given support to the identification of the beam in Her X-1 as having a pencil rather than a fan profile and have scattering optical depth less than 10. However, these inferred optical depths are inconsistent with the pressure and density found in even the simplest dynamical

calculations (Ref. 6, 7). For the luminosities observed in the brighter sources ($L_x > 10^{36}$ erg/sec) the radiation pressure builds to an an extent that it results in a strong radiative deceleration of the inflowing plasma, leading to high densities at the base of the column with scattering optical depths exceeding 10^3. For optical depths exceeding $(m_e c^2/kT_e)^{1/2}$ it is expected that the underlying blackbody spectrum will be substantially Comptonized, resulting in a significant modification of the spectrum, since the scattering opacity in a magnetic field is non-grey (Ref. 7). In addition, the radiative deceleration, where forces due to radiation pressure exceed those due to gravity, lead to inhomogeneities in the accretion column with the result that the source function is inhomogeneous. Since the cross-section is non-grey, the emergent spectrum may show strong departures from a spectrum based upon a uniform model (Ref. 8). Thus, there exists a major need for accretion models that will naturally allow for inhomogeneities in the accretion mound. This requires an equal consideration of both the radiation and the dynamics of the flow. Hence, our goal is to provide a fully self-consistent determination of both the radiation properties of the emitting medium as well as the dynamics of the flow. This necessitates fully time-dependent multi-dimensional coupled radiation-hydrodynamic calculations.

We define the accretion luminosity onto one polar cap to be

$$L_c = \frac{GM_* \dot{M}_c}{R_*} \tag{1}$$

If the Eddington luminosity is defined as

$$L_{ED} = \frac{4\pi\, GM_* mc}{\sigma_T}$$

then we can define the effective Eddington luminosity as in Ref. 10 by

$$L_{ED}^{(eff)} = \frac{A_{cap}}{4\pi R_*^2} H_{\parallel} L_{ED} = \frac{\theta_c^2}{4} H_{\parallel} \frac{4\pi\, GM_* mc}{\sigma_T} \tag{2}$$

where $\sigma_T/H_{\parallel}$ is the angle and frequency averaged cross-section for scattering of radiation flux parallel to B, $\sigma_\perp$ and is the Thomson cross-section and θ_c is the opening angle of the polar cap. The vertical radiation flux leaving the stellar surface at the base of the accretion flow is L_c/A_{cap} when the flow above the star is optically thin and the emission photosphere is on the stellar surface. This optically thin flow can continue only if gravity exceeds the radiation force per particle. Therefore,

$$L_c < L_{ED}^{(eff)}$$

if optically thin flow is to be maintained. However, most of the known X-ray pulsars have

$$L_c > L_{ED}^{(eff)}$$

resulting in optically thick accretion. This leads to a strong coupling of radiation to matter resulting in strong radiation pressure gradients and a halting of freefalling plasma through

much of the accretion column. If we consider characteristic pressures in the accretion column, it is straight forward to show (Ref. 9) that $P_{mag} >> (P_{gas}, P_{dyn}, P_\gamma)$ so that the plasma is easily confined by the magnetic field in the transverse direction and is thus forced to flow along magnetic field lines.

The description of the physics of highly magnetized flow that we have included in our calculations is described in great detail by Arons, Klein and Lea (Ref. 10). Here we consider fully time-dependent, 2-D axi-symmetric radiation hydrodynamics where we have included:

a) magnetically modified bremsstrahlung emission and Coulomb collisional excitation/deexcitation of cyclotron gyration where the cyclotron line emission is treated using a non-L.T.E. 2 Landau level atom with complete redistribution for the resonant scattering. The high optical depth in both the line and the continuum permits us to use the on-the-spot approximation for the cyclotron line transfer.

b) continuum photon-electron energy exchange rate takes account of magnetically modified scattering.

c) the radiation spectrum is essentially a Bose-Einstein distribution with the photon temperature and the photon chemical potential self-consistently determined by a new theory of couple diffusion and advection of both the photon energy density and the photon number density.

d) separate energy equations for the electrons and the ions with full magnetic field modifications.

e) a new flux-limited diffusion theory for transfer of radiation in optically thin, radiation filled structures that are inbedded in optically thick flow.

2. THE EQUATIONS OF RADIATION-HYDRODYNAMICS

Our calculations yield a full space-time evolution of the density $\rho(r,\theta,t)$, velocity $u(r,\theta,t)$, electron energy density $E_e(r,\theta,t)$, ion energy density $E_i(r,\theta,t)$, radiation energy density $E_\gamma(r,\theta,t)$, and photon number density $n_\gamma(r,\theta,t)$. The dominance of magnetic pressure over all other significant pressures enables us to write down the conservation equations in a dipolar geometry where the flow of plasma is constrained to move strictly along the assumed dipole field lines and is not permitted transverse motion. We have

Mass Conservation

$$\frac{\partial}{\partial t}\rho + \frac{1}{r^3}\frac{\partial}{\partial r}\left(r^3 \rho u\right) = 0 \tag{3}$$

Momentum Conservation

$$\frac{\partial}{\partial t}(\rho u) + \frac{1}{r^3}\frac{\partial}{\partial r}\left(r^3 \rho u u\right) = -\rho\frac{GM_*}{r^2} - \frac{\partial}{\partial r}(P_e + P_i) - \frac{\partial P_\gamma}{\partial r} \tag{4}$$

where the total radiation pressure P_γ is the sum of the line and continuum. In the flux limited approximation

$$\frac{\partial P_\gamma}{\partial r} = \frac{D}{3}\frac{\partial}{\partial r}\left(E_{cont} + E_{line}\right) \tag{5}$$

where D is a suitable flux limited coefficient (Ref. 12).

Electron Energy

$$\frac{\partial}{\partial t}(\rho E_e) + \frac{1}{r^3}\frac{\partial}{\partial r}\left(r^3 u \rho E_e\right) + \frac{P_e}{r^3}\frac{\partial}{\partial r}\left(r^3 u\right) = -\Lambda_c - \Lambda_b - \Lambda_l + \Lambda_{ex} \tag{6}$$

Ion Energy

$$\frac{\partial}{\partial t}(\rho E_i) + \frac{1}{r^3}\frac{\partial}{\partial r}\left(r^3 u \rho E_i\right) + \frac{P_i}{r^3}\frac{\partial}{\partial r}\left(r^3 u\right) = -\Lambda_{ex} \tag{7}$$

Radiation Transport

$$\frac{\partial E_\gamma}{\partial t} + \frac{1}{r^3}\frac{\partial}{\partial r}\left(r^3 D E_\gamma u\right) + \frac{E_\gamma}{3}\frac{1}{r^3}\frac{\partial}{\partial r}\left(r^3 D u\right)$$

$$= \Lambda_c + \Lambda_b + \Lambda_l + \frac{1}{r^3}\frac{\partial}{\partial r}\left(\frac{cr^3}{(R+\sigma)_\parallel}\frac{D_\parallel^\varepsilon}{3}\frac{\partial E_\gamma}{\partial r}\right) \tag{8}$$

$$+ \frac{R_*}{\theta r^3}\frac{\partial}{\partial \theta}\left(\frac{\theta c}{(R+\sigma)_\perp}\frac{D_\perp^\varepsilon}{3}\frac{\partial E_\gamma}{\partial \theta}\right)$$

Photon Number Density

$$\frac{\partial n_\gamma}{\partial t} + \frac{1}{r^3}\frac{\partial}{\partial r}\left(r^3 D n_\gamma u\right) = \frac{\Lambda_l}{\varepsilon_b} + \dot{n}_\gamma + \frac{1}{r^3}\frac{\partial}{\partial r}\left(\frac{cr^3}{(K+\sigma)}\frac{D_\parallel^n}{3}\frac{\partial n_\gamma}{\partial r}\right)$$

$$+ \frac{R_*}{\theta r^3}\frac{\partial}{\partial \theta}\left(\frac{\theta c}{(K+\sigma)_\perp}\frac{D_\perp^n}{3}\frac{\partial n_\gamma}{\partial \theta}\right) \tag{9}$$

In the above equations Λ_b is the net bremsstrahlung emission rate, Λ_c is the net rate of Compton energy exchange between photons and elections, Λ_l is the net rate of production of cyclotron line energy, Λ_{EX} is the energy exchange rate between electrons and ions through coulomb encounters and $\dot{n}_\gamma$ is the net production rate for the number of bremsstrahlung photons. In additions $D_\parallel$ and $D_\perp$ are suitably defined diffusion coefficients for directions parallel and perpendicular to the magnetic field.

These equations and the derivations of the physical processes and rates within the equations are described in great detail in Ref. 10.

3. NUMERICAL STRATEGY

We briefly summarize here the approach we take to obtain full solutions of our coupled non-linear P.D.E.'s. The reader should refer to Ref. 11 for a detailed discussion of the techniques used to solve the complete system of radiation- hydrodynamics and a thorough discussion of the inherent difficulties in this complex system.

Hydrodynamics:

We use explicit time-differencing and 2nd order accurate spatial differencing. The hydrodynamics is solved in a two-step operator split procedure. We first advance

$$\rho, \rho u, \rho E_e, \rho E_i, E_\gamma \text{ and } n_\gamma \text{ by } \Delta t$$

using "Lagrangian" terms in the equations.
We next advance

$$\rho, \rho u, \rho E_{lin}, \rho E_i, E_\gamma \text{ and } n_\gamma \text{ by } \Delta t$$

using advective fluxes with Van-Leer monotone advection piece-wise linear 2nd order accurate equations.

Energy Equations:

The equations are implicitly time-differenced with 2nd order accurate spatial differencing using Van-Leer monotone advection for the advective flux terms. The multi-dimensionality is treated with a variation of alternating-direction-implicit operator splitting with all equations using complete linearization to get first order corrections to zeroth order guesses based upon L.T.E. for the first timestep only. The corrections to all variables are consistently iterated to convergence throughout the accretion column for each timestep.

4. RESULTS FOR TWO ACCRETION MODELS

We discuss the results of the first detailed self-consistent multi-dimensional time dependent calculations for accretion onto a highly magnetized neutron star with $B=3\times10^{12}$G. The models have $L_c=3\times10^{37}$ erg/sec with a polar cap opening angle of $\theta_c=0.20$, and $L_c=1.3\times10^{38}$ ergs/sec with $\theta_c=0.15$. Both of these accretion flows represent super-Eddington luminosities with

$L_c = 22L_{ED}^{(eff)}$ for the first model and

$L_c = 175\, L_{ED}^{(eff)}$ for the second model.

The geometry of the accretion flow is shown in Figure 1. We will briefly discuss the evolution of the accretion columns. A detailed discussion of these models will be found in Ref. 11.

In Figure 1 we display the finite difference grid covering the accretion column. Since these are exploratory calculations, we used a grid of 62x21 cells for each model. The geometry of the grid follows the dipole structure of the magnetic field. The center of the neutron star is at (0,0,0) and the polar cap sits on the surface of the star at a radius of 10

km. The height of the accretion column was taken to be 14 km above the surface. Matter is assumed to flow into the top of the accretion column uniformly across the accretion column at a rate

$$\dot{M}_c = R_* L_c / GM_* .$$

The initial conditions were chosen so that the incoming plasma is in free-fall throughout the accretion column with a velocity

$$u = \left(\frac{2GM_*}{R_*}\right)^{1/2} \left(\frac{R_*}{r}\right)^{1/2}$$

and a corresponding density

$$\rho = \frac{1}{u} \frac{\dot{M}_c}{A_{cap}} \left(\frac{R_*}{r}\right)^3$$

The plasma is assumed initially cold with a temperature Te=Ti=5×10^6 and a radiation energy density calculated from L.T.E. conditions. The lower boundary assumes no radiative or mechanical flux into the star. The upper boundary assumes a uniform mass accretion flux into the accretion column and a freely radiating surface. The central field line has zero radiative flux by symmetry and the outermost field line (the edge of the accretion column) has a freely radiating surface.

At t=2.4×10^{-5} s. a strong accretion shock has formed on the stellar surface and a dense crust covers the polar cap. The optically thick flow traps the thermalized radiation as the photon diffusion time exceeds the photon advection time, thus radiation is essentially dragged downward toward the stellar surface more rapidly than it can diffuse and finds its only exit through a fan beam out the side of the accretion column. This is clearly seen in Figure 2 which represents the radiative flux vectors. In the central region of the accretion column we note the downward advection of the radiation, whereas at the sides the radiation escapes as a fan beam. Contours of the velocity field at this time for the higher luminosity case $L_c=1.3\times10^{38}$ erg/sec are shown in Figure 3. The dashed contours represent outward flowing plasma and the solid contours represent inflowing plasma. The radiation dominated shock that has formed in the shape of a mound just above the stellar surface greatly impedes the inflowing matter from free- fall velocities u=0.5c to u=10^{-4}c. The radiation pressure force inside the radiation dominated accretion mound has increased enough to turn the incoming plasma into a slight outflow. At t=3.3×10^{-4} s. (Figure 4) the uniform outflow region of earlier times has become a more complex series of disconnected outflow rolls in the flow. We believe this is the onset of a form of overstable convection (Ref. 12) as the plasma develops low density regions giving rise to a net buoyancy force. In Figure 5 we see the flux for both models at t=4.0×10^{-4} s. A well formed fan beam ring has formed around the accretion column about 1 Km above the surface. The velocity of the plasma at this time (Figure 6) indicates that one of the outflow regions has disappeared in the high luminosity case and a small outflow region has come into existence in the lower luminosity case. Evidently, the outflow regions are very dynamic entities that are capable of forming and re-forming. At t=5.4×10^{-4} s.(Figure 7) the single outflow region near the axis has reformed further out in the accretion column for the $L_c=1.3\times10^{38}$ case, while for lower luminosities, the initial outflow has grown substantially and a second outflow structure has appeared. These outflow regions embed regions of very low density, and radiation easily leaks into these regions which exhibit substantially lower optical depth than the surrounding optically thick plasma. This migration of the radiation into these low density "holes" in the accretion column is seen in Figure 8 at t=7.0×10^{-4} s.where we begin to see evidence of the formation of photon bubbles. The density in these bubbles $\rho = 3\times10^{-7}$ surrounded by matter of considerably higher density. The velocity structure in the lower luminosity case (Figure 9) shows two very well developed photon bubble outflow

regions surrounded by inflowing plasma that has been radiatively decelerated to velocities considerably less than free fall with a free-fall region at the edge of the column extending to the surface of the star. The $L_c=1.3\times10^{38}$ case now shows evidence of a second photon bubble forming outside the first. At $t=9.1\times10^{-4}$ s.(Figure 10) the $L_c=3.0\times10^{37}$ case shows the dramatic growth of the dominant photon bubble as the radiation pushes sideways causing outflow throughout most of the accretion column and resulting in the merging of the two bubble structures into one. The higher luminosity case now begins the development of a third photon bubble. In Figure 11 at $t=1.1\times10^{-3}$ s. we note that although a fan beam component of radiation remains out the side of the accretion column, much of the radiation in the interior of the column moves into the low density "holes" created by the photon bubbles. As the radiation fills these "holes" clearly seen in the density contours in Figure 12 we note that the density structure in the column becomes highly inhomogeneous with evacuated regions with $\rho = 5.6\times10^{-8}$ surrounded by inflow regions with $\rho = 2.2\times10^{-4}$. At the edge of the column where free-fall is still possible, high density regions form, giving densities $\rho = 1.6\times10^{-1}$ g/cm^{3}for the lower luminosity case and $\rho = 1.34$ g/cm^3 for the high luminosity case. In Figure 13 we see that the photon bubbles have completely merged in the lower luminosity case to form one very dominant photon bubble structure leading to outflow throughout most of the accretion column. In the high luminosity case, we note the development of four distinct photon bubble structures. These outflow regions are embedded in inflow regions of substantially decelerated inflow. The photon bubble merger in the $L_c=3\times10^{37}$ case is most likely due to the lower optical depth in the walls encasing these bubbles than for the $L_c=1.3\times10^{38}$ case. Thus, the radiation from adjacent bubbles can leak from one such structure to another leading to bubble merger. In the higher luminosity case, the photons are trapped in bubbles surrounded by optically thicker plasma and the bubbles are more likely to remain distinct. It is clear that the development of these dominant outflow regions lead to completely inhomogeneous structure in the accretion columns. This in turn results in highly inhomogeneous radiation source functions showing the inadequacy of previous one zone uniform models in describing the conditions inside the accretion column.

In Figure 14, we note the photon bubble development at $t=1.2510^{-3}$ s. The outflow region has reached the upper boundary of the accretion column. A substantial region of the accretion column is in outflow bounded above and to the side by radiatively decelerated inflow and free-fall at the edge. The large outflowing region itself is complex contain within it several small regions that are actually accreting matter down onto the stellar surface. Thus, the topology of the accretion column for high luminosity accretion flows consists mainly of three distinct regions; i) outflowing photon bubbles, ii) inflowing shock decelerated matter and iii) free-fall near the edge. This distinct topology results in a very inhomogeneous structure as can be seen in the density contours in Figure 15, indicating strong departures from previously assumed uniform accretion columns. This inhomogeneity implies that the emitted spectrum will sample contributions to the source function from patches of the accretion mound with widely ditfering physical resulting in a spectrum that can significantly depart from that calculated assumed homogeneity in the column.

The radiation flux shown in Figure 16 shows the tendency for the radiation to be carried up through the accretion column in the photon bubble structures. It should be pointed out that the upper boundary is at scattering optical depth $\tau=7$, thus the radiation will not yet be observable. This is a consequence of not having removed the upper boundary far enough from the stellar surface. This will be rectified in further calculations. The potential for photon bubbles to turn into pencil beam components has great significance for X-ray pulsars like Her X-1. Observations of the pulse profiles have suggested that this system can best be explained as having a pencil beam. It has long been assumed that uniform accretion columns could only give rise to fan beam radiation patterns, and so Her

X-1 must in fact be an example of hollow cone type accretion. Our preliminary calculations indicate that both pencil and fan beam components of the emitted radiation may be possible even for uniform accretion as a natural consequence of buoyant photon bubble structures present in the highly inhomogeneous accretion column. In Figures 1 and 18 we show the calculated luminosity as a function of time out the side of the accretion column and up through the accretion column respectively. The total luminosity out the side of the column reaches 17% of the accretion luminosity $L_c=3\times10^{37}$. The luminosity up through the top of the accretion column however, is 83% of the accretion luminosity. The growth time for the maximum luminosity is about 10^{-3} s. and the light curves indicate fluctuations on sub-millisecond times scales. These preliminary calculations indicate the enticing possibility that photon bubbles which have growth times 10^{-3} s. and fluctuations with sub-millisecond periods may carry most of the radiated energy up through the accretion column and turn into a pencil beam profile while still maintaining a less significant fan beam component with significantly less emitted energy. Further calculations are required to establish that the radiation carried up through the column by a photon bubble structure can indeed give rise to a pencil beam.

5. DISCUSSION

Detailed time-dependent, 2-D, self-consistent radiation-hydrodynamical calculations have been made to follow the evolution of the dynamical and radiative structure of the accretion column of high luminosity X-ray pulsars. We have, for the first time, found the existence of unstable low-density outflowing regions that are filled with radiation (photon bubbles) with photon temperature $T_\gamma \sim 10$ Kev and are surrounded by very optically thick inflowing plasma. These photon bubbles are highly dynamical as they form, merge with other bubbles disappear and re-form. These photon bubble structures move through the accretion column subsonically. We are currently performing calculations that will elucidate the fate of these bubbles. Of great interest is how the bubbles will dispose of the radiative energy they contain. It is possible the bubbles will deposit their energy through the top of the accretion column as a radiative jet, deliver bursts of radiation that will appear as a series of sub-millisecond fluctuations in the light curve, go into a limit cycle mode, or appear as a chaotic percolative phenomenon.

The photon bubbles are a form of overstable convection. The instability is not the same as was looked at by Spiegel (Ref. 13) several years ago but does have similarities. He specifically assumed bulk transport of the photon enthalpy is negligible; but for the effects considered here, it is essential over a wide range of frequency. The linear growth of the instability can be studies analytically. The details will be presented elsewhere.

The equilibrium model used to study the instability is a simplification of the steady flow model of Arons and Klein (Ref. 9). The density and radiation pressure are both exponentially stratified with pressure

$$p_\gamma = p_* e^{-z/h} \tag{10}$$

and density

$$\rho_0 = \rho_* e^{-z/h} \tag{11}$$

Thus, the equilibrium generalized sound speed

$$c_{so} = \sqrt{4p_\gamma/3\rho_o} \tag{12}$$

is a constant. The variation of p_γ and of ρ_0 with distance across the field is neglected. The equilibrium flow velocity is obtained from mass conservation $\rho_0 v_0 = f$, with f a constant. The scale height comes from the diffusion convection model for the flow,

$$h = \frac{c}{v_o}\lambda_s = \frac{L_{ED}^{(eff)}}{L_c} R_* = \frac{3c_{s0}^2}{4g} \tag{13}$$

If the disturbances to the pressure, density and velocity change in proportion to $\exp(\Gamma t)$, and it is assumed the only dissipation process is isotropic Thomson scattering, described in the diffusion approximation then in the WKB limit, when the wavelength is small compared to h, the result for Γ is

$$\Gamma = i(kh)\frac{v_o}{h}\left(\frac{4}{9}\tan^2\theta - \cos\theta\right) + \frac{9}{16}\left(\frac{v_o}{c_{s0}}\right)^2 (kh)^2 \frac{v_o}{h}\tan^4\theta\,. \tag{14}$$

Thus, we have an overstable oscillation. It actually depends directly on the diffusivety of the radiation. This is hidden in equation (14) because the mean free path is eliminated in favor of the scale height h using equation (13).

Evaluation of Γ yields a growth rate comparable to the rate of formation of "photon bubbles" observed in our non-linear numerical simulations. As an illustration, consider the following evaluation. From (4), we have

$$c_{s0}^2 = \frac{4}{3}\frac{GM}{R_*^2}\frac{L_{ED}^{(eff)}}{L_c} R_* = \frac{2}{3} v_{esc}^2 \frac{L_{ED}^{(eff)}}{L_c}\,. \tag{15}$$

For a neutron star of radius 10 km and mass 1 $M_\odot$, and an accretion luminosity 100 times the effective Eddington luminosity (5×10^{37} ergs/s onto the pole, if magnetic corrections to the opacity are neglected), the sound speed is $c_{s0} = 1.3 \times 10^4$ km/s. A typical velocity in the polar accretion flow is $v_0 = 3000$ km/s. The scale height from equation (13) is 100 meters. Then the dynamic time h/v_0 is 33 μsec, and Γ yields

$$\Re(\Gamma) = 0.9 \times 10^3 (kh)^2 \tan^4\theta\ s^{-1}.$$

For $\tan\theta \leq 1$, which is required by the transverse stratification not included in the calculation, and $kh \sim 1$, which is implied by the expectation that the largest buoyancy modes eventually control the flow, we find growth times in the millisecond regime, consistent with the time scales for formation of the photon bubbles. In addition, oscillations in the initial growth are predicted with frequency

$$G(\Gamma) \sim \frac{v_o}{h} = 3 \times 10^4\left(\frac{4}{9}\tan^2\theta - 1\right) s^{-1}.$$

These oscillations with growth times $\frac{1}{G(\Gamma)} \sim$ sub-millisecond

are indeed present in the emitted luminosity (Figure 17, 18). We believe the luminosity fluctuations are connected to oscillations with this period in the velocity, density, temperature, etc.

A question of extreme importance is whether or not any steady state actually exists for super-Eddington flows? To begin to address this problem we used the analytic steady state solutions recently obtained by Arons and Klein (Ref. 9) as initial conditions for the full time-dependent calculations. The analytic steady state solution indicates a radiative mound solution with Gaussian stratification in radiation and density across the accretion column and an exponential stratification along the magnetic field, with the radiative shock bounding the mound close to the stellar surface. However, this solution appears not to remain steady once the time-dependence is allowed to turn on. Preliminary results suggest that the mound blows out forming a large photon bubble region looking significantly different than the analytic steady state. While our first results indicate that the steady state is not a true equilibrium, these are not yet firm conclusions and we must do much additional work to show conclusively that a true steady state may not exist. This is discussed in more detail in Ref. 11.

6. SUMMARY

- For super-Eddington flows
  $\left(L_{cap} > L_{ED}^{(eff)}\right)$,
  accretion columns are highly inhomogeneous. This may result in a substantial modification of the emitted spectrum from that predicted by previous uniform slab models.

- We have discovered evidence of the formation of photon bubbles in the accretion models for high luminosity x-ray pulsars. These outflowing low density regions have growth times on the order of a millisecond and show preliminary evidence of fluctuations through the luminosity on sub-millisecond timescales. These timescales are consistent with results from a linear stability analysis which suggests the bubbles form as a form of convective overstability. The photon bubbles have the potential of carrying significant bursts of radiation up through the accretion column. Preliminary calculations indicate that this mechanism may indeed give us a pencil beam component for the pulse profile even when accretion occurs with a uniform mass inflow. This may have significant implications for systems like Her X-1, thought to be a pencil beam where it is usually assumed that only hollow cone accretion can account for the beaming. Photon bubbles may be observable as fluctuations in the light curve and luminosity dependent changes in the pulse profile. This could provide an important new diagnostic probe of the structure of the accretion column.

- We find for $L_c = 3\times10^{37}$ erg/sec, photon bubbles merge as radiation conducts easily through the bubble walls. For $L_c = 1.3\times10^{38}$, where the flow is considerably more optically thick, multiple bubbles form and remain distinct.

- Analytic steady state mound models may not remain steady in time. Preliminary results indicate a significant departure from a steady solution. Thus, super-Eddington flows may not have a steady state. This would include most of the x-ray pulsars.

- The lack of presence of cyclotron lines in most x-ray pulsars may be due to severe doppler shifts in highly inhomogeneous accretion columns.

- We find that $T_e \approx T\gamma \sim 10$ keV in the accretion column. A fan beam of radiation forms with a height of 1 km. above the stellar surface.

- We find that cyclotron line production of photons >10 bremsstrahlung emission.

- A self-consistent calculation of the photon chemical potential $\mu\gamma = 0$ (L.T.E.) throughout the center of the accretion column. We find substantial departures ($\mu\gamma \neq 0$) of the radiation from L.T.E. at the top and sides of the column.

ACKNOWLEDGEMENTS

This research was performed under the auspices of NSF grant AST-8615816 and the U.S. Department of Energy by the Lawrence Livermore National Laboratory under Contract W-7405-Eng-48, and the taxpayers of the State of California.

REFERENCES

1. Pringle, J. E., and Rees, M. J., 1972, Astr. Ap., 21, 1.
2. Davidson, K., Ostieker, J. P., 1973, Ap.J., 179, 585.
3. Lamb, F. K., Pethick, C. J. and Pines, D., 1973, Ap.J., 184, 271.
4. Meszaros,, P., 1984, in High Energy Transients in Atrophysics, ed. S.E. Wooseley (New York: AIP), p. 165.
5. Mezaros, P., and Nagel, W., 1985, Ap.J., 298, 147.
6. Davidson, K., 1973, Nature Phys. Sci., 246, 1
7. Basko, M. M., and Sunyaev, R. A., 1976, M.N.R.A.S., 175, 395.
8. Burnard, D., Arons, J., and Klein, R. I., 1990, submitted to Ap.J.
9. Arons. J. and Klein, R. I., 1990, In preparation.
10. Arons, J., Klein, R. I., and Lea, S. M., 1987, Ap.J., 312, 666.
11. Klein, R. I. and Arons, J., 1990, In preparation.
12. Proctor, M., and Weiss, N., 1982, Rep. Prog. Phys. 45, 1317.
13. Spiegel, E. ., 1976, In Physics of the Motion of Stellar Atmospheres, p. 19, International Colloquim, CNRS, Nice; Ed. Cayrel and Steinberg.

Figure Captions:

Figure 1. Computational Grid; Stellar surface at 10^6 cm.

Figure 2. Radiation flux at $t=2.4\times10^{-5}$ s.

Figure 3. Velocity Field at $t=2.4\times10^{-5}$ s. Dashed contours are outflowing velocities, solid contours are inflowing.

Figure 4. Velocity contours at $t=3.3\times10^{-4}$ s.

Figure 5. Radiation flux at t=4.0x10-4 s. Upper plot shows $L_c = 3.0\times10^{37}$; lower is for $L_c = 1.3\times10^{38}$.

Figure 6. Velocity at $t=4.0\times10^{-4}$ s. for both models.

Figure 7. Velocity field at $t=5.4\times10^{-4}$ s. for both models.

Figure 8. Radiation flux at $t=7.0\times10^{-4}$ s. for both models.

Figure 9. Velocity field at $t=7.0\times10^{-4}$ s. for both models.

Figure 10. Velocity field at $t=9.1\times10^{-4}$ s. for both models.

Figure 11. Radiation flux at $t=1.1\times10^{-3}$ s. for both models.

Figure 12. Density contours at $t=1.1\times10^{-3}$ s. for both models.

Figure 13. Velocity field at $t=1.1\times10^{-3}$ s. for both models.

Figure 14. Velocity field at $t=1.25\times10^{-3}$ s. for $L_c = 3\times10^{37}$.

Figure 15. Density contours at $t=1.25\times10^{-3}$ s. for $L_c = 3\times10^{37}$.

Figure 16. Radiative flux at $t=1.25\times10^{-3}$ s. for $L_c = 3\times10^{37}$.

Figure 17. Total luminosity vs. time from side of the accretion column. Time is in units of 10^{-3} s., luminosity is in units of 10^{36} erg/sec.

Figure 18. Total luminosity vs. time from top of accretion column. Time is in units of 10^{-3} s., luminosity is in units of 10^{37} erg/sec.

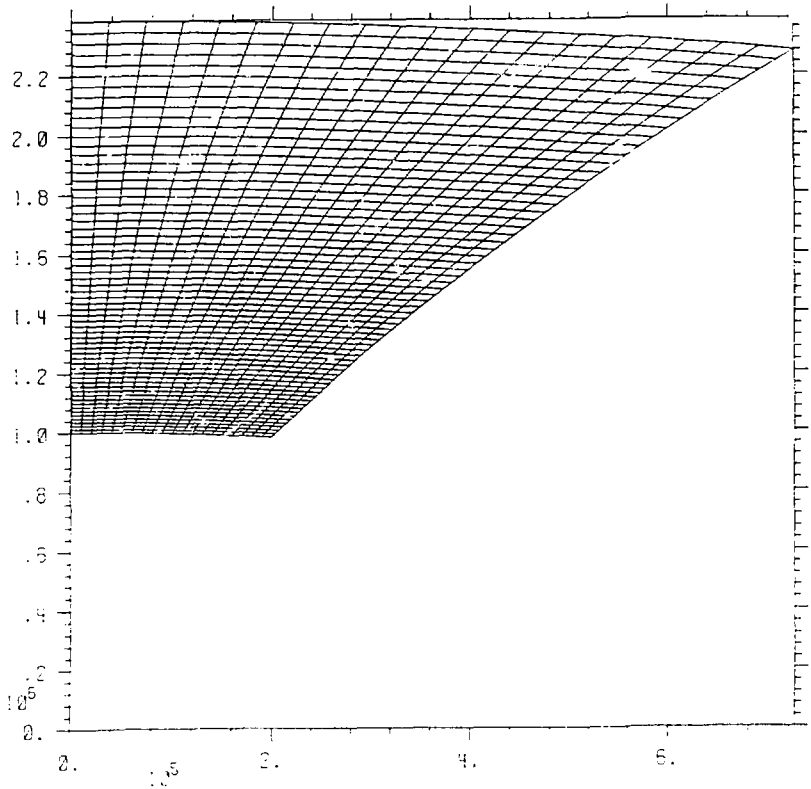

Figure 1 - Computational Grid, stellar surface at 10^6 cm.

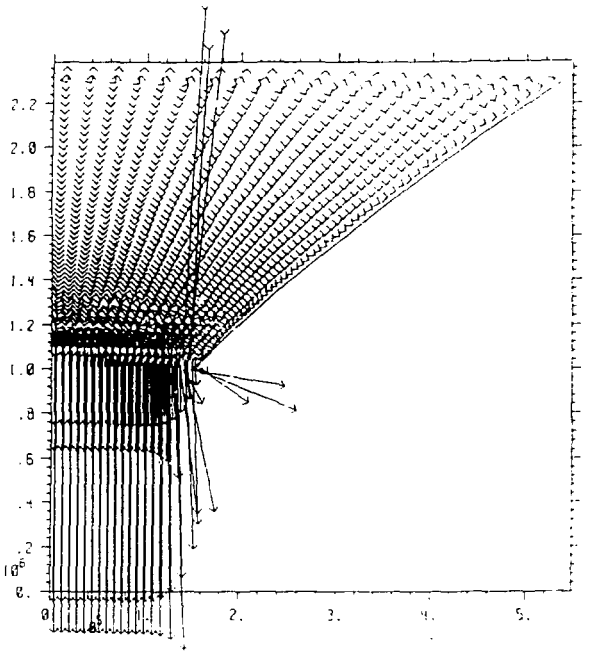

Figure 2. Radiation flux at $t=2.4\times10^{-5}$ s.

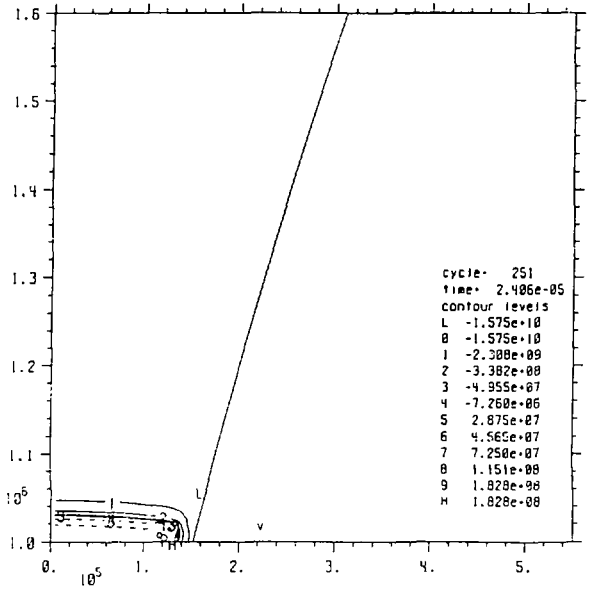

Figure 3. Velocity Field at $t=2.4\times10^{-5}$ s. Dashed contours are outflowing velocities, solid contours are inflowing.

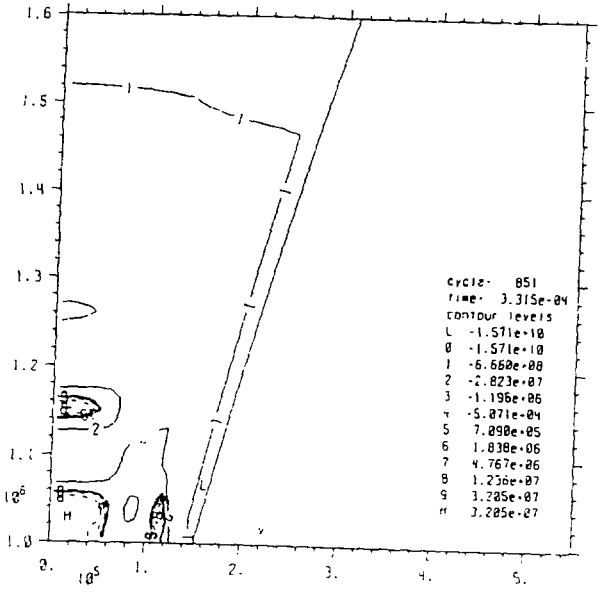

Figure 4. Velocity contours at $t=3.3\times10^{-4}$ s.

Figure 5. Radiation flux at t=4.0x10-4 s. Upper plot shows $L_c = 3.0 \times 10^{37}$; lower is for $L_c = 1.3 \times 10^{38}$.

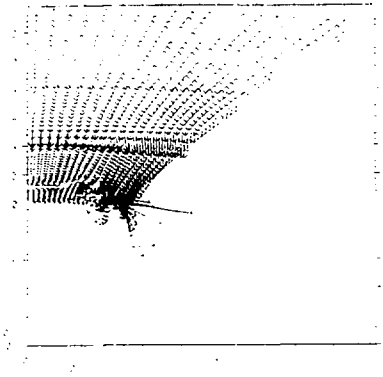

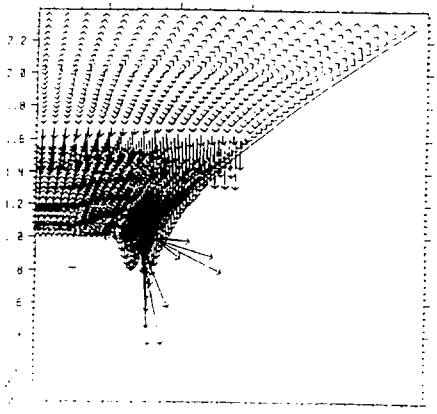

Figure 6. Velocity at $t=4.0\times10^{-4}$ s. for both models.

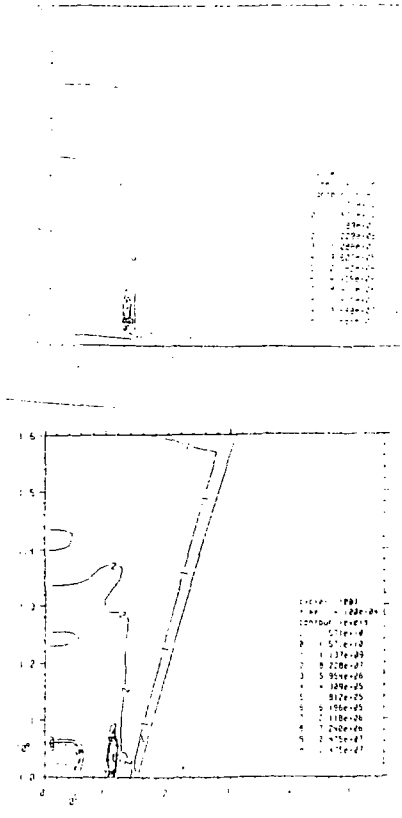

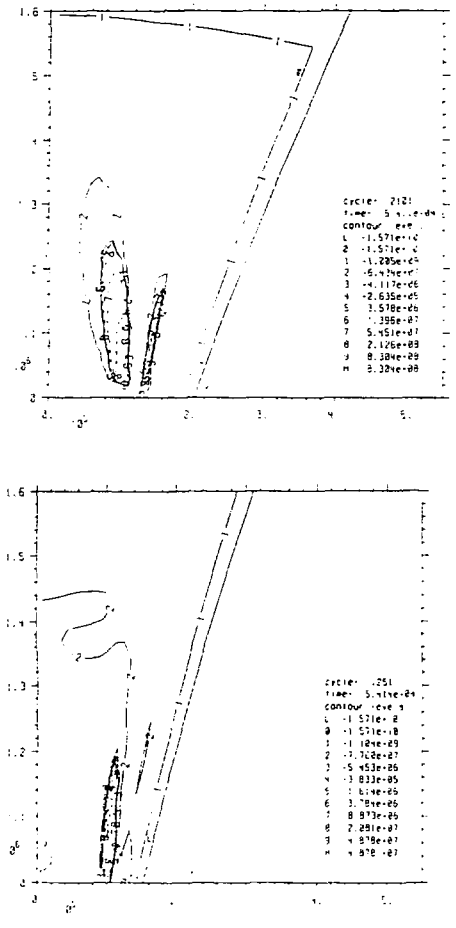

Figure 7. Velocity field at $t=5.4\times10^{-4}$ s. for both models

Figure 8. Radiation flux at $t=7.0\times10^{-4}$ s. for both models.

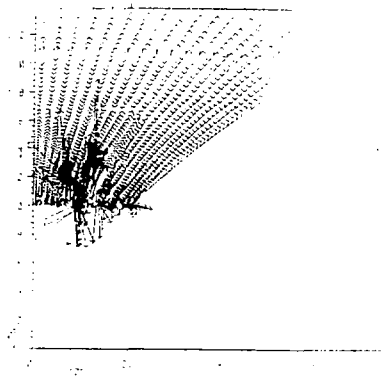

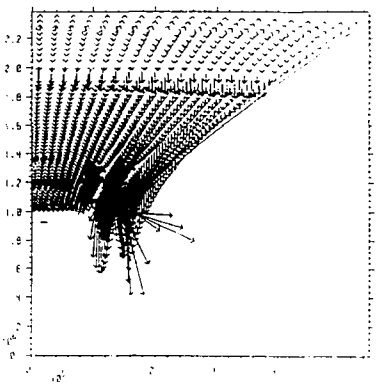

Figure 9. Velocity field at $t=7.0\times10^{-4}$ s. for both models.

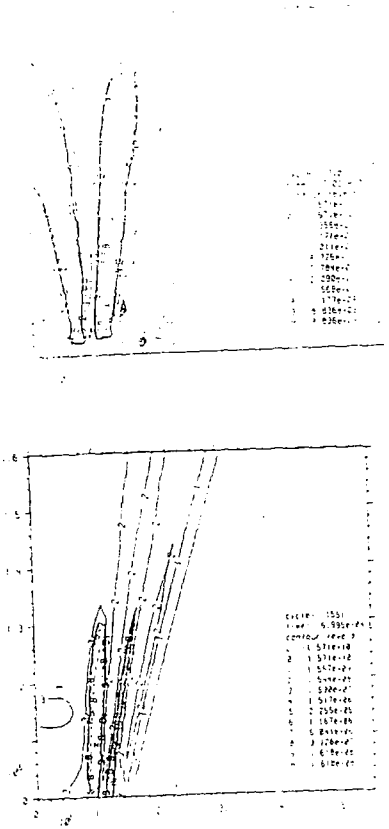

Figure 10. Velocity field at $t=9.1\times10^{-4}$ s. for both models.

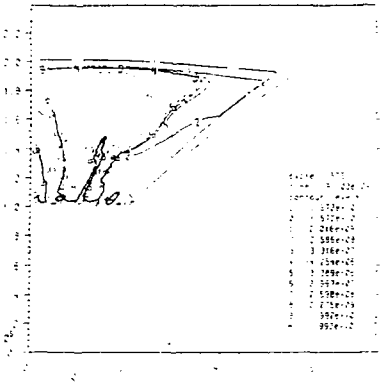

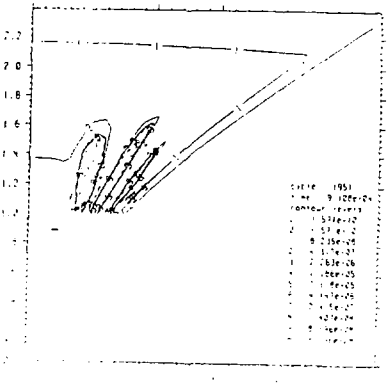

Figure 11. Radiation flux at $t=1.1\times10^{-3}$ s. for both models.

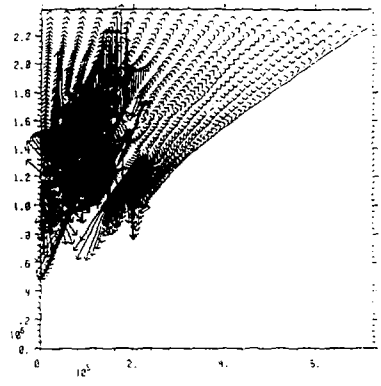

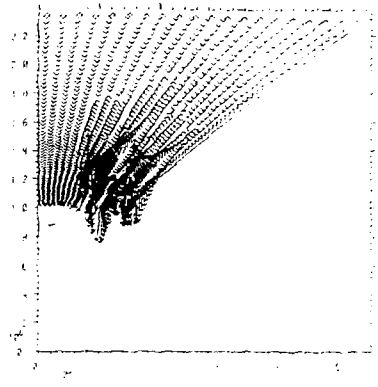

Figure 12. Density contours at $t=1.1\times10^{-3}$ s. for both models.

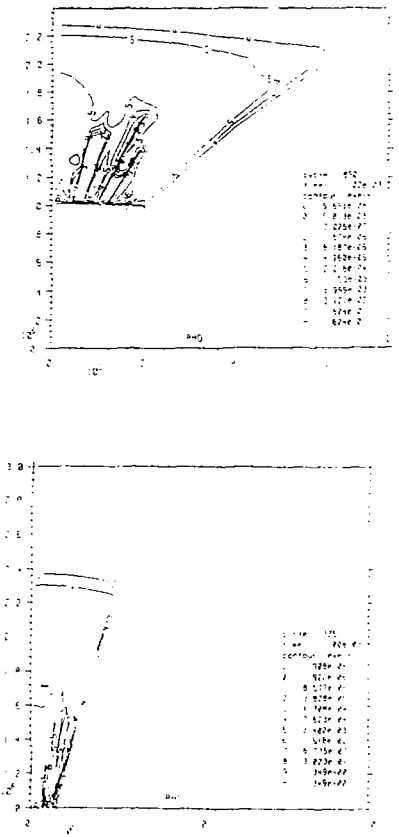

Figure 13. Velocity field at $t=1.1\times10^{-3}$ s. for both models.

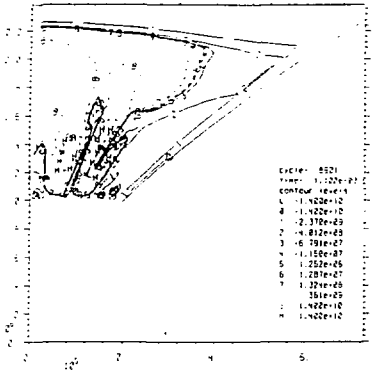

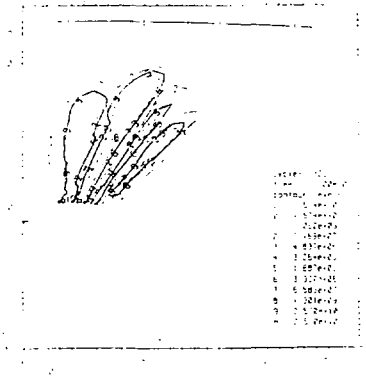

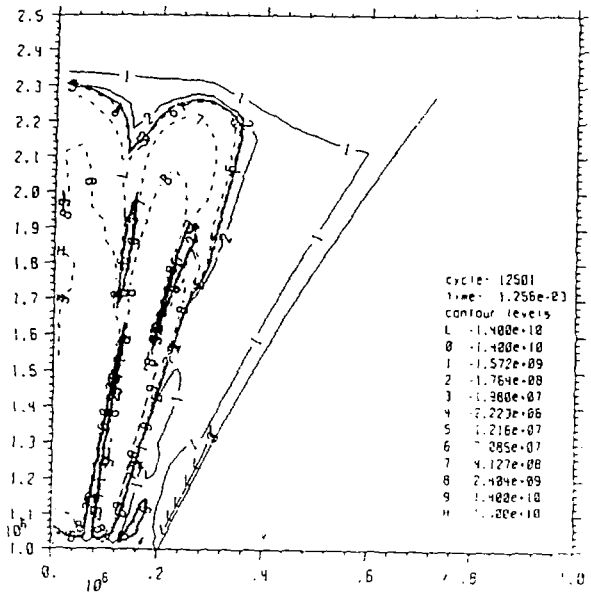

Figure 14. Velocity field at $t \approx 1.25 \times 10^{-3}$ s. for $L_c = 3 \times 10^{37}$.

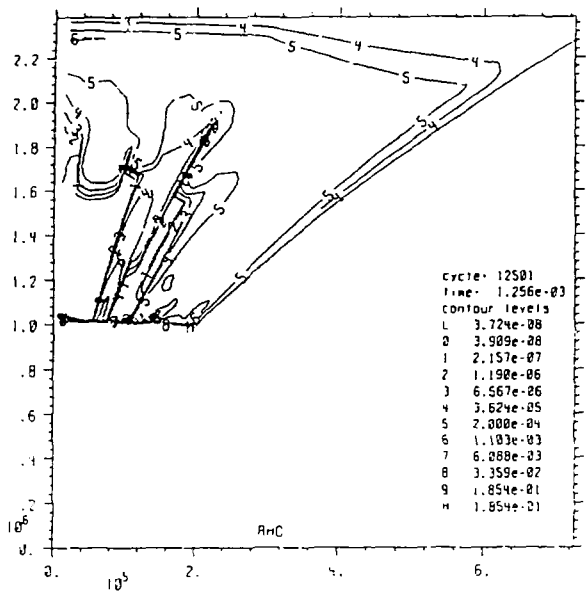

Figure 15. Density contours at $t=1.25\times10^{-3}$ s. for $L_c = 3\times10^{37}$.

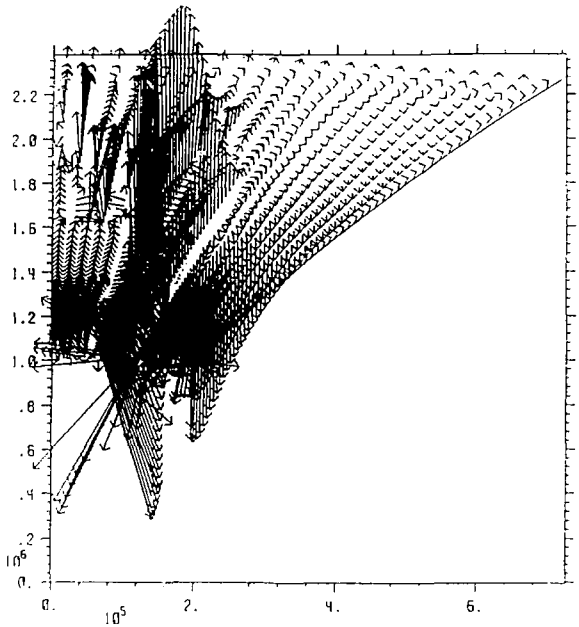

Figure 16. Radiative flux at $t=1.25\times10^{-3}$ s. for $L_c = 3\times10^{37}$.

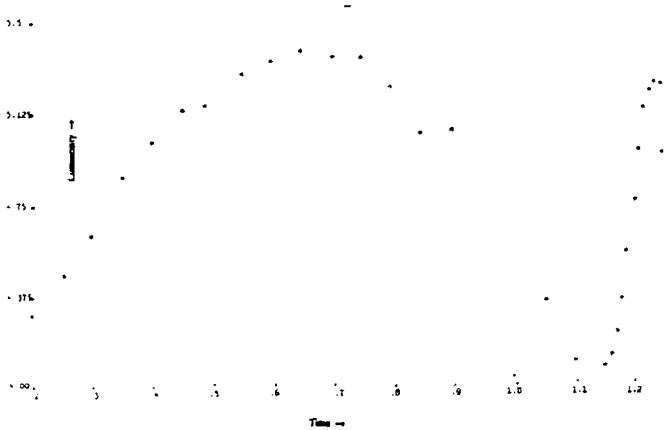

Figure 17 Total luminosity vs. time from onset of the supernova explosion. Time is in units of 10^{-3} s, luminosity is in units of 10^{50} erg/sec.

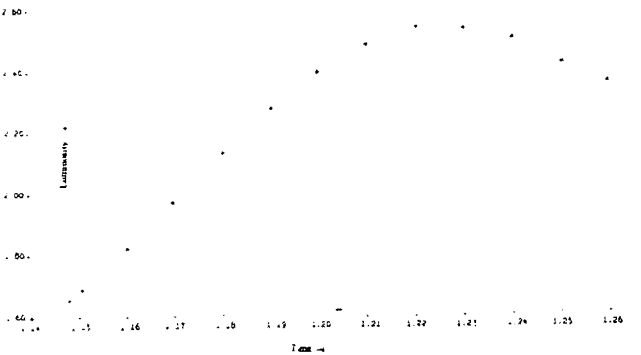

Figure 18 Total luminosity vs. time from top of supernova collapse. Time is in units of 10^{-3} s., luminosity is in units of 10^{51} erg/sec.